Hindawi
International Journal of Aerospace Engineering
Volume 2022, Article ID 2761275, 17 pages
https://doi.org/10.1155/2022/2761275

Research Article

Prescribed Performance Adaptive Control for a Nonlinear Aeroelastic System with Input Constraint

Zijun Gao, Junjie Zhang, Jiaqi Li, and Zhankui Song

School of Information Engineering, Dalian Polytechnic University, 116034, China

Correspondence should be addressed to Zijun Gao; gaozijun_dpu@163.com

Received 5 October 2021; Revised 30 January 2022; Accepted 9 March 2022; Published 1 April 2022

Academic Editor: Kenneth M. Sobel

A constrained prescribed performance compensation controller is proposed for a nonlinear aeroelastic system in the presence of wind gust, system uncertainties, and input saturation. To deal with the effects of the nonsmooth saturation nonlinearity, an approximate saturation function is introduced into the controller design, which can smoothly approximate the real saturation with arbitrarily prescribed precision. Specifically, by designing the prescribed performance function, a fixed-time control framework is designed to ensure that the closed-loop system has the prescribed tracking performance. The designed control algorithm can not only compensate the adverse effect caused by disturbances and uncertainties but also restrain the excessive amplitude of control input. Finally, the stability analysis shows that all the signals in the closed-loop system are semiglobally uniformly ultimately bounded via the Lyapunov stability analysis method, and simulation results are presented to demonstrate the feasibility and effectiveness of the proposed method.

1. Introduction

Recent developments in aeroelasticity research and the aeroelastic system control design have attracted increasing attention and concern among scientists and practitioners [1–5]. In aeroelastic systems, the limit cycle oscillation is an important problem and is usually associated with flutter, which can degrade the performance of aerospace vehicles and dramatically affect flight safety. Therefore, it is particularly important to develop a reliable and effective control method to solve such problems. In previous studies [6–8], researchers have analyzed the nonlinear responses of aeroelastic systems, and various advance control approaches have been extensively studied in the field of flutter and limit cycle oscillation suppression.

In order to obtain an effective controller, a full feedback linearization controller based on two control surfaces was designed in [9], and the stability of the closed-loop aeroelastic system was further investigated. A high-order sliding mode controller [10] was proposed for suppressing limit cycle oscillation with a backstepping design. The state-dependent Riccati equation method was developed for nonlinear control problems and used to design suboptimal control laws of nonlinear aeroelastic systems considering both quasisteady [11, 12] and unsteady aerodynamics [13, 14]. In aeroelastic systems, parameter uncertainties and external disturbances are unavoidable [15]; if these problems cannot be compensated and dealt with in time, the relevant performances of the aeroelastic system are likely to be greatly affected and even cause system instability. To the best of the authors' knowledge, adaptive nonlinear control approach is an effective way to solve the above problem. In [16], an adaptive decoupled fuzzy sliding-mode controller was employed for aeroelastic system to achieve system tracking stabilization. Wang et al. [17] proposed an output feedback adaptive controller for achieving the fine tracking performance of MEMS. In [18], an adaptive robust control scheme with input constraints was proposed for MEMS to improve the antidisturbance ability. Thereafter, an adaptive super-twisting continuous control method [19] and adaptive sliding mode controller with neural network observer [20] were developed for multi-input and multioutput aeroelastic system with unsteady aerodynamics in the presence of uncertainty and gust loads. Recently, an effective function

estimator using the interval type-2 and type-3 fuzzy logic system has been extensively studied for adaptive control. Based on this function estimation technique, some new adaptive nonlinear control strategies [21, 22] were devised to tackle the effects of perturbations and estimation errors.

Although the studies mentioned above can achieve the corresponding control objectives, some important control performance cannot be guaranteed to be determined in advance. For special control tasks, the desired control performances (such as convergence speed, overshoot, and steady-state error) are needed to be set in the early stage of control and realized during the control process. The urgent need for preset performance of control systems drives the development of nonlinear control methods. An effective solution strategy called the prescribed performance constraint method was proposed in [23–26], which is easily designed a predefined prescribed performance bound to characterize the convergence rate and the maximum overshoot of tracking error such that the desired transient performance can be achieved. Based on the prescribed performance strategy, many nonlinear control methods have also been extended and applied to various nonlinear systems [27–33]. It is worth mentioning that the above-mentioned control methods are derived in the sense of Lyapunov asymptotic stability, which means that the system error reaches a residual set in infinite time rather than fixed time, and moreover, it is not easy to calculate the residual set size due to unknown bounded terms.

Control input saturation is another issue that needs to be considered in aeroelastic systems, which is also a source of performance degradation. In the past few years, some compensation methods have been proposed for solving input saturation problem in various nonlinear systems [34–38]. In [39], a sliding mode controller using the auxiliary system was developed for attitude tracking of quadrotor with input constraints. Unfortunately, the fixed-time prescribed performance cannot be achieved by the proposed control system. In [40], a predefined-time prescribed performance control approach was designed for spacecraft rendezvous with input saturation, but system parameters (the inertia matrix of pursuer) were considered as the nominal parameters.

Despite the progress in the research on anti-input saturation [34–40], it should be noticed that little attention has been paid on the fixed-time prescribed performance control for coexistence problem of system parameter uncertainties and input constraints. Therefore, it is still a challenging open issue to improve control performance and robustness for adverse factors including parameter uncertainty and input constraints.

Motivated by the above discussion, an input constrained control scheme is proposed for the aeroelastic system with wind gust and system uncertainties in this paper. The main features of this paper are briefly summarized as follows:

(1) By designing the fixed-time performance function, a control method with built-in time and error constraint mechanism is proposed to ensure that the tracking errors converge to a prescribed compact set within a fixed time

(2) The proposed control law is compatible with the control input saturation suppression algorithm that naturally fulfills the magnitude limits by designing an input updating law. Under the framework of the proposed control strategy, it is proved by theory that all internal signal variables are bounded

(3) The designed control strategy does not need to know the precise information of the system model, and the proposed settling time is independent of the initial conditions

The rest of this paper is organized as follows. Section 2 introduces the aeroelastic model and gives the problem description. A fixed-time prescribed performance controller with saturation suppression algorithm and the stability analysis are presented in Section 3. The effectiveness of the proposed strategy is verified by simulation in Section 4. Finally, conclusions are given in section 5.

2. Problem Formulation and Preliminaries

2.1. System Description. The prototype aeroelastic wing with leading and trailing edge surfaces is shown in Figure 1. The aeroelastic system has two degrees of freedom, one is the plunge displacement h, and the other is the pitch angle α. In the presence of a flow field, the wing at a flight speed U oscillates along the plunge displacement direction and rotates at the pitch angle about the elastic axis [1].

The dynamics of the aeroelastic system is described by [4, 5]

$$\begin{bmatrix} I_\alpha & m_w x_\alpha b \\ m_w x_\alpha b & m_t \end{bmatrix} \begin{bmatrix} \ddot{\alpha} \\ \ddot{h} \end{bmatrix} + \begin{bmatrix} c_\alpha & 0 \\ 0 & c_h \end{bmatrix} \begin{bmatrix} \dot{\alpha} \\ \dot{h} \end{bmatrix} + \begin{bmatrix} k_\alpha(\alpha) & 0 \\ 0 & k_h \end{bmatrix} \begin{bmatrix} \alpha \\ h \end{bmatrix} = \begin{bmatrix} M \\ -L \end{bmatrix} + \begin{bmatrix} M_g \\ -L_g \end{bmatrix}. \tag{1}$$

Here, aerodynamic lifts (L and L_g) and moments (M and M_g) are given as

$$L_g = \mu\, U\, b\, s\, c_{l\alpha} w_G(t_r), \tag{2}$$

$$M_g = (0.5 - a) \cdot b \cdot L_g, \tag{3}$$

$$L = \mu U^2 b s c_{l_\alpha} \left(\alpha + \frac{\dot{h}}{U} + \left(\frac{1}{2} - a \right) \frac{b\dot{\alpha}}{U} \right) + \mu U^2 b s \left(c_{l\beta}\beta + c_{l_\gamma}\gamma \right), \tag{4}$$

$$M = \mu U^2 b^2 s \left\{ \left(\frac{c_{l\alpha}}{2} + a c_{l\alpha} + 2c_{m\alpha} \right) \left(\alpha + \frac{\dot{h}}{U} + \left(\frac{1}{2} - a \right) \frac{b\dot{\alpha}}{U} \right) \cdot \left[\left(\frac{c_{l\beta}}{2} + a c_{l\beta} + 2c_{m\beta} \right) \beta + \left(\left(\frac{1}{2} + a \right) c_{l\gamma} + 2c_{m\gamma} \right) \gamma \right] \right\}. \tag{5}$$

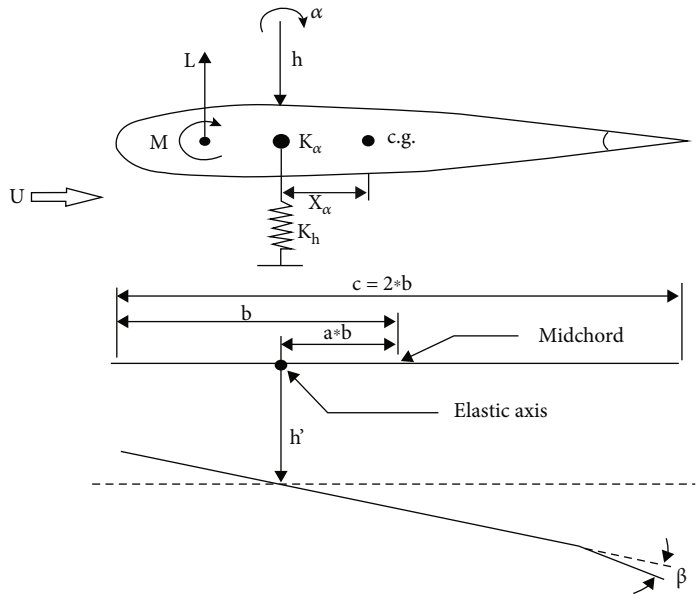

Figure 1: Aeroelastic model.

Note that γ and β are the trailing edge and the leading edge control surface deflections, respectively.

To facilitate understanding of the specific meanings of system parameters, the relevant symbol descriptions in Equations (1) and (2) are presented in Table 1. Considering that there are many system parameters in (1), some hybrid parameters are defined in Table 2 for the convenience of analysis. It should be pointed out that these hybrid parameters are not fully known; moreover, $b_{ij}(i = 1, 2\,; j = 1, 2)$ can be decomposed into nominal $\bar{b}_{ij}$ and uncertain parts Δb_{ij}, i.e., $b_{ij} = \bar{b}_{ij} + \Delta b_{ij}$.

Let $x_1 = \alpha$, $x_2 = \dot{\alpha}$, $x_3 = h$, $x_4 = \dot{h}$, $u_1 = \bar{b}_{11}\beta + \bar{b}_{12}\gamma$, and $u_2 = \bar{b}_{21}\beta + \bar{b}_{22}\gamma$, for $i = 1, 2$; the aeroelastic system (1) can be written as

$$\begin{cases} \dot{x}_{2i-1} = x_{2i}, \\ \dot{x}_{2i} = f_i + u_i, \end{cases} \tag{6}$$

where $f_1 = d_1 - k_3x_3 - c_3x_4 - (k_4U^2 + p_2)x_1 + \Delta b_{11}\beta - (c_4 + q_2)x_2 + \Delta b_{12}\gamma$ and $f_2 = d_2 - k_1x_3 - c_1x_4 + \Delta b_{21}\beta - (k_2U^2 + p_1)x_1 - (c_2 + q_1)x_2 + \Delta b_{22}\gamma$.

In practical applications, the control input should be limited within a reasonable range due to the physical constraints. Considering that the trailing edge and leading edge control surface of the aeroelastic wing have maximum deflection limits, therefore, there exist the maximum bounds and $\beta_{\max}$ such that $|\gamma| \le \gamma_{\max}$ and $|\beta| \le \beta_{\max}$. Furthermore, by combining $u_1 = \bar{b}_{11}\beta + \bar{b}_{12}\gamma$ and $u_2 = \bar{b}_{21}\beta + \bar{b}_{22}\gamma$, for $i = 1, 2$, we can obtain that

$$u_i = \begin{cases} \text{sign}\,(\tau_i) \cdot u_{iM} & \text{if} |\tau_i| \ge \tau_{iM}, \\ \tau_i & \text{if} |\tau_i| < \tau_{iM}, \end{cases} \tag{7}$$

where τ_i are needed to be designed, $\tau_{1M} = \bar{b}_{11}\beta_{\max} + \bar{b}_{12}\gamma_{\max}$, and $\tau_{2M} = \bar{b}_{21}\beta_{\max} + \bar{b}_{22}\gamma_{\max}$.

Obviously, u_i are the saturation functions which can lead to nonsmooth control action near the saturation limit. Thus, we introduce the following smooth function $\Gamma_{\tau_{iM}}(\tau_i)$ proposed in [41] to approximate the saturation functions (7). (A comparison of the three saturated nonlinear functions is shown in Figure 2.)

$$\Gamma_{\tau_{iM}}(\tau_i) = \frac{1}{2c} \ln\left(\frac{e^{c\tau_{iM}}e^{c\tau_i} + e^{-c\tau_{iM}}e^{-c\tau_i}}{e^{-c\tau_{iM}}e^{c\tau_i} + e^{c\tau_{iM}}e^{-c\tau_i}}\right), \tag{8}$$

where $c > 0$ and $\tau_{iM} > 0$ are the design parameters.

Lemma 1 (see [41]). *The saturation functions $u_i(i = 1, 2)$ in (7) can be expressed as*

$$u_i = \Gamma_{\tau_{iM}}(\tau_i) + \Delta\tau_i, \tag{9}$$

and the following properties hold.

P1: $(\partial\Gamma_{\tau_{iM}}(\tau_i)/\partial\tau_i) > 0$.

P2: $\Delta\tau_i$ *are bounded and* $\lim_{c\longrightarrow+\infty} \Delta\tau_i = 0$.

P3: $|\Gamma_{\tau_{iM}}(\tau_i)| \le \tau_{iM}$.

Proof. See the appendix. □

With the aid of Lemma 1, it follows from (6) that

$$\begin{cases} \dot{x}_{2i-1} = x_{2i}, \\ \dot{x}_{2i} = D_i + \Gamma_{\tau_{iM}}(\tau_i), \end{cases} \tag{10}$$

where $D_i = f_i + \Delta\tau_i$. To construct the control system, the following assumptions are needed.

Table 1: Nomenclature.

Symbol	Description
m_w	Mass of the wing
h	Plunging displacement
α	Pitch angle about the pitch axis
I_α	Inertial moment of the wing about the elastic axis
m_t	Total mass of the wing and its support structure
x_α	Dimensionless distance between the center of mass and elastic axis
a	Nondimensional distance from airfoil midchord to elastic axis
k_α	Pitch stiffness
k_h	Plunge stiffness
M	Aerodynamic moment
L	Aerodynamic lift
$c_{l\alpha}$	Derivatives of aerodynamic lift coefficient ($c_{l\beta}$ and c_{ly} have the similar definitions)
M_g	Aerodynamic moment due to gust
L_g	Aerodynamic force duet to gust
c_h	Plunge damping
c_α	Pitch damping
μ	Air density
b	Airfoil semichord
s	Wing section span
β	Angle of trailing edge
γ	Angle of leading edge
U	Free stream velocity
w_G	Disturbance velocity
$c_{m\alpha}$	Moment derivatives ($c_{m\beta}$ and $c_{m\gamma}$ have the similar definitions)

Table 2: Hybrid parameter definition.

Definition
$k_1 = I_\alpha k_h / \left(m_t I_\alpha - (m_w x_\alpha b)^2\right)$
$k_2 = \left(I_\alpha \mu b s c_{l\alpha} + m_w x_\alpha b^3 \mu s c_{m\alpha}\right) / \left(m_t I_\alpha - (m_w x_\alpha b)^2\right)$
$k_3 = -m_w x_\alpha b k_h / \left(m_t I_\alpha - (m_w x_\alpha b)^2\right)$
$k_4 = \left(m_w \mu s x_\alpha b^2 c_{l\alpha} + m_t b^2 \mu s c_{m\alpha}\right) / \left(m_t I_\alpha - (m_w x_\alpha b)^2\right)$
$p_1 = m_w x_\alpha b k_\alpha / \left((m_w x_\alpha b)^2 - m_t I_\alpha\right)$
$p_2 = m_t k_\alpha / \left(m_t I_\alpha - (m_w x_\alpha b)^2\right)$
$c_1 = \left[I_\alpha (c_h + \mu s U b c_{l\alpha}) + m_w \mu s U x_\alpha b^3 c_{m\alpha}\right] / \left(m_t I_\alpha - (m_w x_\alpha b)^2\right)$
$c_2 = \left[\left(I_\alpha + \mu s U b^2 c_{l\alpha} m_w \mu s U x_\alpha b^4 c_{m\alpha}\right)(0.5 - a) + \right] / \left(m_t I_\alpha - (m_w x_\alpha b)^2\right)$
$c_3 = m_w \left(x_\alpha b c_h + x_\alpha \mu U b^2 c_{l\alpha} + \mu U b^2 c_{m\alpha}\right) / \left((m_w x_\alpha b)^2 - m_t I_\alpha\right)$
$c_4 = \left[\left(m_w x_\alpha \mu U b^3 c_{l\alpha} + m_t \mu U b^2 c_{m\alpha}\right)(0.5 - a)\right] / \left((m_w x_\alpha b)^2 - m_t I_\alpha\right)$
$q_1 = m_w x_\alpha b c_\alpha / \left((m_w x_\alpha b)^2 - m_t I_\alpha\right)$
$q_2 = m_t c_\alpha / \left(m_t I_\alpha - (m_w x_\alpha b)^2\right)$
$b_{11} = U^2 \mu s m_w x_\alpha b^2 c_{l\beta} + m_t b^2 \left((0.5 + a) c_{l\beta} + 2 c_{m\beta}\right)) / \left(m_t I_\alpha - (m_w x_\alpha b)^2\right)$
$b_{12} = U^2 \mu s \left(m_w x_\alpha b^2 c_{l\gamma} + m_t b^2 ((0.5 + a)) c_{l\gamma} + 2 c_{m\gamma}\right)) / \left(m_t I_\alpha - (m_w x_\alpha b)^2\right)$
$b_{21} = U^2 \mu s \left(I_\alpha b c_{l\beta} + m_w x_\alpha b^3 ((0.5 + a)) c_{l\beta} + 2 c_{m\beta}\right)) / \left((m_w x_\alpha b)^2 - m_t I_\alpha\right)$
$b_{22} = U^2 \mu s \left(I_\alpha b c_{l\gamma} + m_w x_\alpha b^3 s ((0.5 + a)) c_{l\gamma} + 2 c_{m\gamma}\right)) / \left((m_w x_\alpha b)^2 - m_t I_\alpha\right)$
$d_1 = \left(m_t M_g (m_w x_\alpha b) \cdot L_g\right) / \left(I_\alpha m_t - (m_w x_\alpha b)^2\right)$
$d_1 = \left(I_\alpha L_g (m_w x_\alpha b) \cdot M_g\right) / \left((m_w x_\alpha b)^2 - I_\alpha m_t\right)$

Assumption 2. The nonlinear functions $D_i (i = 1, 2)$ are bounded by unknown constant δ_D, i.e., $|D_i| \le \delta_D$.

Assumption 3. The physical states of system are bounded and remain in a set Z, i.e.,

$$Z = \left\{ \alpha, \dot{\alpha}, h, \dot{h} \,\middle|\, |\alpha| \le \alpha^{\max}, |\dot{\alpha}| \le \bar{\alpha}^{\max}, |h| \le h^{\max}, |h| \le \bar{h}^{\max} \right\}, \tag{11}$$

where $\alpha^{\max}$, $\bar{\alpha}^{\max}$, $h^{\max}$, and $\bar{h}^{\max}$ are the upper bound values of the corresponding variables.

Assumption 4. The desired command signals $x_{(2i-1)d} (i = 1, 2)$ and their derivative $\dot{x}_{(2i-1)d}$ and $\ddot{x}_{(2i-1)d}$ are bounded.

Assumption 5. The system states x_{2i-1}, x_{2i}, and $\dot{x}_{2i} (i = 1, 2)$ can be measured by physical sensors.

Remark 6. The synthetic functions $D_i (i = 1, 2)$ in (10) contain several parameters related to the aeroelastic system. In fact, these parameters are all bounded, which means that there is also an upper bound for $\max \{|D_1|, |D_2|\}$. Considering the limited energy of the airflow vibration and the physical constraints of the aeroelastic system, hence, α, $\dot{\alpha}$, h, and $\dot{h}$ are bounded. In addition, the system states can be obtained by physical sensors (for example, x_{2i-1} can be measured from the laser positioning sensor, and x_{2i} and $\dot{x}_{2i}$ can be measured from gyroscope sensor integrated by a 3-axis MEMS accelerometer and a digital motion processor). Based on the analysis above, Assumptions 2-5 are valid. The similar assumptions can be found in [38]. It should be pointed out that the bounds of these parameters are not involved in the design of the control law.

2.2. Preliminaries. To study the control performance of the closed loop system, the following definition is required.

Definition 7 (see [42, 43]). A smooth function $\rho(t)$ is called the fixed-time performance function if there exist the preassigned time T_S and preset precision ρ_{TS} such that

(1) $\rho(t) > 0$ and $\dot{\rho}(t) \le 0$ for $\forall t \in [0, T_S)$

(2) $\rho(t) = \rho_{TS} > 0$ for $\forall t \ge T_S$

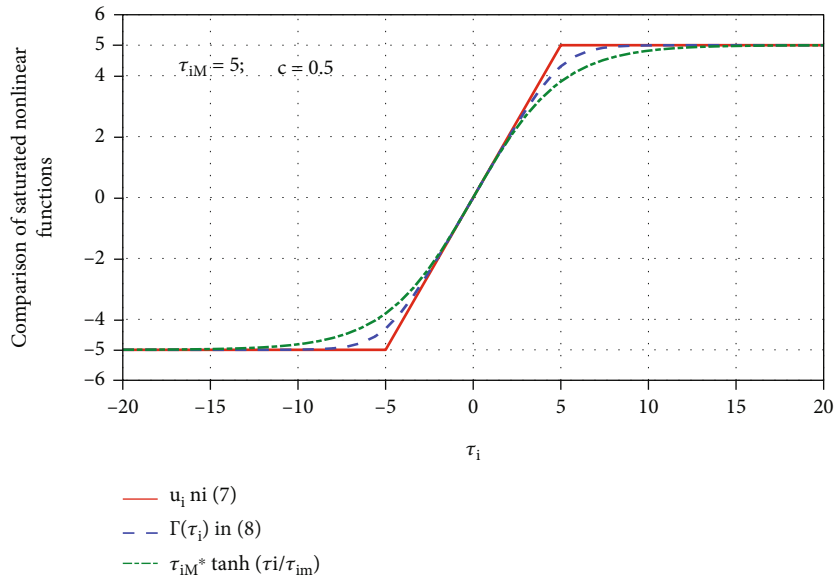

Figure 2: Comparison of saturated nonlinear functions.

Based on the above definition, the fixed-time performance functions $\rho_i(i = 1, 2)$ [44] are constructed as

$$\rho_i(t) = \begin{cases} -\frac{\bar{\rho}}{3T_S^3}t^3 + \frac{\bar{\rho}}{T_S^2}t^2 - \frac{\bar{\rho}}{T_S}t + \rho_0, & \text{for } t \in [0, T_S), \\ \rho_{TS}, & \text{for } t \in [T_S, \infty), \end{cases} \tag{12}$$

where $\bar{\rho} = 3(\rho_0 - \rho_{TS})$ with positive constant ρ_0. From (12), it easily follows that $\dot{\rho}_i(t) < 0$ for $t \in [0, T_S)$, $\rho_i(t) = \rho_{TS} > 0$ for $t \in [T_S, \infty)$, $\lim_{t \to T_S^-}(\rho_i(t) - \rho_i(T_S))/(t - T_S) = \lim_{t \to T_S^+}(\rho_i(t) - \rho_i(T_S))/(t - T_S) = 0$, and $\lim_{t \to T_S^-}\rho_i(t) = \lim_{t \to T_S^+}\rho_i(t) = \rho_{TS}$. Then, we have

$$\dot{\rho}_i(t) = \begin{cases} -\frac{\bar{\rho}}{T_S^3}t^2 + \frac{2\bar{\rho}}{T_S^2}t - \frac{\bar{\rho}}{T_S}, & \text{for } t \in [0, T_S), \\ 0, & \text{for } t \in [T_S, \infty). \end{cases} \tag{13}$$

The change trend of the performance function $\rho(t)$ is presented in Figure 3. In this paper, $\rho(t)$ is used to restrain and schedule the convergence trend of the system errors. Notice that the selection of the fixed-time T_S in $\rho(t)$ cannot be arbitrarily small and it should be larger than the sampling time.

In this paper, the control objective is to design a fixed-time prescribed performance control scheme for system (10), such that the system errors converge to a prescribed compact set within a fixed time T_S.

3. Main Results

We now propose the fixed-time prescribed performance control method for the aeroelastic system. The concrete design procedure is given as follows:

Step 1. Define the system tracking errors as follows:

$$\begin{cases} e_{2i-1} = x_{2i-1} - x_{(2i-1)d}, \\ e_{2i} = x_{2i} - \varphi_i, i = 1, 2. \end{cases} \tag{14}$$

Here, φ_i are the virtual control laws which will be designed later. Combining with (10) and the definition of e_{2i}, the time derivative of e_{2i-1} can be found as

$$\dot{e}_{2i-1} = \dot{x}_{2i-1} - \dot{x}_{(2i-1)d} = e_{2i} + \varphi_i - \dot{x}_{(2i-1)d}. \tag{15}$$

Next, the virtual control laws are designed as

$$\varphi_i = -\kappa_{2i-1} \cdot e_{2i-1} + \dot{x}_{(2i-1)d} + \frac{e_{2i-1}\dot{\rho}_i}{\rho_i}, \tag{16}$$

in which κ_{2i-1} are positive design parameters. Substituting φ_i into (15) yields

$$\dot{e}_{2i-1} = e_{2i} - \kappa_{2i-1} \cdot e_{2i-1} + \frac{e_{2i-1}\dot{\rho}_i}{\rho_i}. \tag{17}$$

Step 2. Define the auxiliary deviation variables as

$$\begin{cases} s_i = \Gamma_{\tau_{iM}}(\tau_i) - \Gamma_{\bar{\varphi}_{iM}}(\bar{\varphi}_i), \\ \Delta\bar{\varphi}_i = \Gamma_{\bar{\varphi}_{iM}}(\bar{\varphi}_i) - \bar{\varphi}_i, i = 1, 2, \end{cases} \tag{18}$$

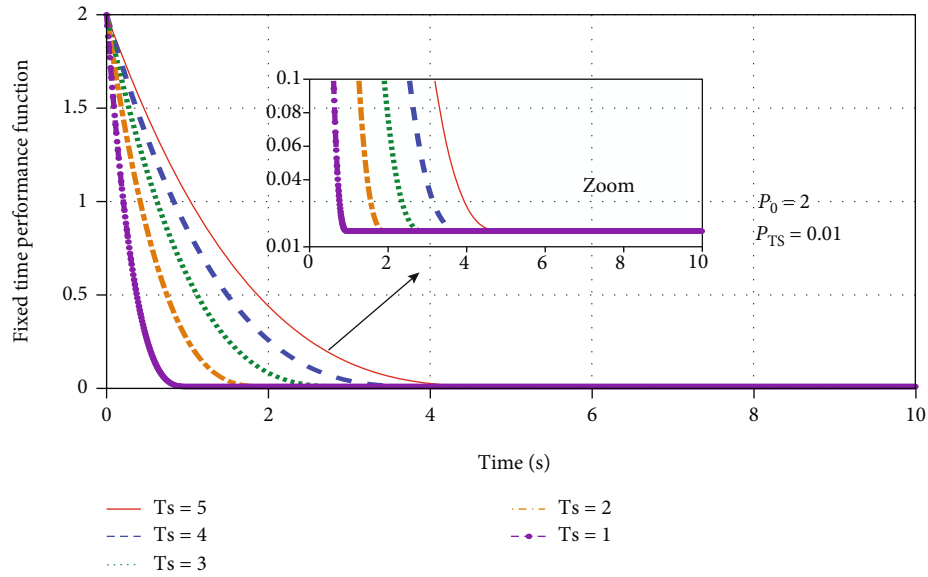

(a) The dynamic diversification curves with different T_S

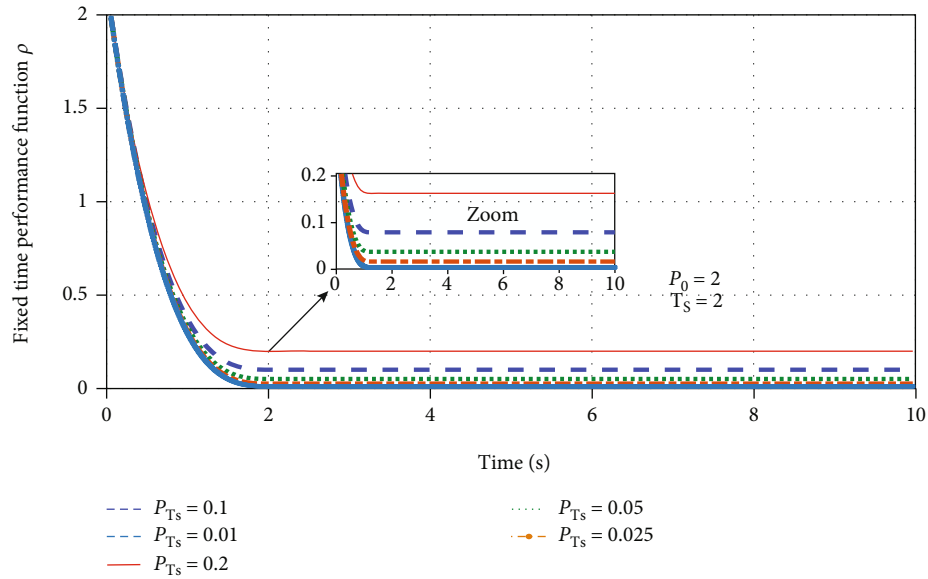

(b) The dynamic diversification curves with different ρ_{TS}

FIGURE 3: The dynamic diversification curves of $\rho(t)$.

where τ_i are updated by (30); $\Gamma_{\bar{\varphi}_{iM}}(\bar{\varphi}_i)$ and $\bar{\varphi}_i$ are given as

$$\Gamma_{\bar{\varphi}_{iM}}(\bar{\varphi}_i) = \frac{1}{2c} \ln\left(\frac{e^{c\bar{\varphi}_{iM}} e^{c\bar{\varphi}_i} + e^{-c\bar{\varphi}_{iM}} e^{-c\bar{\varphi}_i}}{e^{-c\bar{\varphi}_{iM}} e^{c\bar{\varphi}_i} + e^{c\bar{\varphi}_{iM}} e^{-c\bar{\varphi}_i}}\right), \tag{19}$$

$$\bar{\varphi}_i = -\frac{\widehat{\sigma}_i \cdot e_{2i}}{2a_1^2} - \kappa_{2i} \cdot e_{2i} - \frac{e_{2i-1}}{\rho_i^2 - e_{2i-1}^2}. \tag{20}$$

In (19) and (20), κ_{2i} and a_1 are the positive design parameters; $\bar{\varphi}_{iM} = 0.5c^{-1} \ln\left((e^{c(2\tau_{iM}-\varepsilon)} + e^{-c(2\tau_{iM}-\varepsilon)})/(e^{-c\varepsilon} + e^{c\varepsilon})\right)$ with constant ε satisfying $\tau_{iM} > \varepsilon > 0$; in addition, $\widehat{\sigma}_i$ are updated by

$$\dot{\widehat{\sigma}}_i = \xi_i \cdot \left(\frac{-a_1 \cdot \widehat{\sigma}_i + e_{2i}^2}{2a_1^2}\right) \quad (\xi_i > 0, \widehat{\sigma}_i(0) = 0). \tag{21}$$

It should be pointed out that s_i (in (18)) are introduced into the control system design to avoid the excessive amplitude of τ_i. The elimination mechanism of excessive control amplitude will be given later.

Remark 8. According to the function properties of (19), we can obtain that $\Gamma_{\bar{\varphi}_{iM}}(\bar{\varphi}_i)$ are bounded, i.e., $|\Gamma_{\bar{\varphi}_{iM}}(\bar{\varphi}_i)| \leq \bar{\varphi}_{iM}$.

Therefore, we can further prove that

(1) if $\tau_i \geq \tau_{iM} - \varepsilon$, it can be obtained from the properties of $\Gamma_{\tau_{iM}}(\tau_i)$ that $\Gamma_{\tau_{iM}}(\tau_i) \geq \Gamma_{\tau_{iM}}(\tau_{iM} - \varepsilon) > 0$. Notice that

$$\begin{aligned} &\Gamma_{\tau_{iM}}(\tau_{iM} - \varepsilon) = \frac{1}{2c} \cdot \ln\left(\frac{e^{c(2\tau_{iM}-\varepsilon)} + e^{-c(2\tau_{iM}-\varepsilon)}}{e^{-c\varepsilon} + e^{c\varepsilon}}\right), \\ &\left|\Gamma_{\bar{\varphi}_{iM}}(\bar{\varphi}_i)\right| \leq \bar{\varphi}_{iM} = \frac{1}{2c} \cdot \ln\left(\frac{e^{c(2\tau_{iM}-\varepsilon)} + e^{-c(2\tau_{iM}-\varepsilon)}}{e^{-c\varepsilon} + e^{c\varepsilon}}\right). \end{aligned} \tag{22}$$

Using the fact $\bar{\varphi}_{iM} = (1/2c) \ln\left((e^{c(2\tau_{iM}-\varepsilon)} + e^{-c(2\tau_{iM}-\varepsilon)})/(e^{-c\varepsilon} + e^{c\varepsilon})\right)$, then

$$\begin{aligned} s_i &= \Gamma_{\tau_{iM}}(\tau_i) - \Gamma_{\bar{\varphi}_{iM}}(\bar{\varphi}_i) \geq \Gamma_{\tau_{iM}}(\tau_{iM} - \varepsilon) - \bar{\varphi}_{iM} \\ &= \frac{1}{2c} \ln\left(\frac{e^{c(2\tau_{iM}-\varepsilon)} + e^{-c(2\tau_{iM}-\varepsilon)}}{e^{-c\varepsilon} + e^{c\varepsilon}}\right) - \bar{\varphi}_{iM} = 0. \end{aligned} \tag{23}$$

(2) if $\tau_i \leq -\tau_{iM} + \varepsilon$, it implies that $\Gamma_{\tau_{iM}}(\tau_i) \leq \Gamma_{\tau_{iM}}(-\tau_{iM} + \varepsilon) < 0$

Since

$$\begin{aligned} \Gamma_{\tau_{iM}}(-\tau_{iM} + \varepsilon) &= \frac{1}{2c} \ln\left(\frac{e^{c\varepsilon} + e^{-c\varepsilon}}{e^{-c(2\tau_{iM}-\varepsilon)} + e^{c(2\tau_{iM}-\varepsilon)}}\right), \\ \bar{\varphi}_{iM} &= -\frac{1}{2c} \ln\left(\frac{e^{-c\varepsilon} + e^{c\varepsilon}}{e^{c(2\tau_{iM}-\varepsilon)} + e^{-c(2\tau_{iM}-\varepsilon)}}\right), \end{aligned} \tag{24}$$

therefore, we have

$$\begin{aligned} s_i &= \Gamma_{\tau_{iM}}(\tau_i) - \Gamma_{\bar{\varphi}_{iM}}(\bar{\varphi}_i) \leq \Gamma_{\tau_{iM}}(-\tau_{iM} + \varepsilon) + \bar{\varphi}_{iM} \\ &= \frac{1}{2c} \ln\left(\frac{e^{c\varepsilon} + e^{-c\varepsilon}}{e^{-c(2\tau_{iM}-\varepsilon)} + e^{c(2\tau_{iM}-\varepsilon)}}\right) + \bar{\varphi}_{iM} = 0. \end{aligned} \tag{25}$$

Combining with the analysis above, we obtain

$$\begin{cases} s_i \geq 0, & \text{if } \tau_i \geq \tau_{iM} - \varepsilon, \\ s_i \leq 0, & \text{if } \tau_i \leq -\tau_{iM} + \varepsilon. \end{cases} \tag{26}$$

From (14) and (18), the derivative of e_{2i} and s_i is calculated as follows:

$$\begin{cases} \dot{e}_{2i} = \dot{x}_{2i} - \dot{\bar{\varphi}}_i = D_i + \Gamma_{\tau_{iM}}(\tau_i) - \dot{\bar{\varphi}}_i = s_i + \bar{\varphi}_i + \Psi_i, \\ \dot{s}_i = \dfrac{\partial \Gamma_{\tau_{iM}}(\tau_i)}{\partial \tau_i} \cdot \dot{\tau}_i - \dfrac{\partial \Gamma_{\bar{\varphi}_{iM}}(\bar{\varphi}_i)}{\partial \bar{\varphi}_i} \cdot \dot{\bar{\varphi}}_i, \end{cases} \tag{27}$$

where $\Psi_i = D_i + \Delta\bar{\varphi}_i - \dot{\varphi}_i$. Before the main result is given, a compact sets is defined as

$$\Omega = \left\{ e_{2i-1}, e_{2i}, s_i \middle| \sum_{i=1}^{2} \left(\frac{\rho_i^2}{\rho_i^2 - e_{2i-1}^2} + e_{2i}^2 + s_i^2 \right) \leq \vartheta, (\vartheta \in \mathbb{R}^+) \right\}. \tag{28}$$

Obviously, there must be the point corresponding to the supreme value of Ψ_i in $\Omega \times Z$, such that

$$\Psi_i^2 \leq \sigma_i \quad (i = 1, 2), \tag{29}$$

where $\sigma_i > 0$ are the unknown constants.

Remark 9. Notice that Ψ_i contain the uncertain function terms D_i, which make it impossible to directly add the uncertain function to eliminate itself in the controller design. In the stability analysis, the upper bound of Ψ_i^2 can be displayed through inequality scaling under the help of (29), and furthermore, the upper bound of Ψ_i^2 can be estimated and compensated by designing the online adaption laws $\hat{\dot{\sigma}}_i$ in (21). Based on this processing method, the stability of the closed-loop system can be guaranteed by the proposed control strategy.

Next, the input updating laws are designed as follows:

$$\dot{\tau}_i = \begin{cases} \left[\dfrac{\partial \Gamma_{\tau_{iM}}(\tau_i)}{\partial \tau_i}\right]^{-1} \cdot \left[\omega_i - \dfrac{1}{2}\left(1 + \omega_i^2\right)\right], & \text{if } \tau_i \geq \tau_{iM} - \varepsilon, \\ \left[\dfrac{\partial \Gamma_{\tau_{iM}}(\tau_i)}{\partial \tau_i}\right]^{-1} \cdot \omega_i, & \text{if } |\tau| < \tau_{iM} - \varepsilon, \\ \left[\dfrac{\partial \Gamma_{\tau_{iM}}(\tau_i)}{\partial \tau_i}\right]^{-1} \cdot \left[\omega_i + \dfrac{1}{2}\left(1 + \omega_i^2\right)\right], & \text{if } \tau \leq -\tau_{iM} + \varepsilon, \end{cases} \tag{30}$$

where $\tau_i(0) = 0$ and $\omega_i = (\partial \Gamma_{\bar{\varphi}_{iM}}(\bar{\varphi}_i)/\partial \bar{\varphi}_i) \cdot \dot{\bar{\varphi}} - \kappa_{2i} s_i - e_{2i}$.

Remark 10. In view of (16), we have $\dot{\varphi}_i = -\kappa_{2i-1}\dot{e}_{2i-1} + \ddot{x}_{(2i-1)d} + (\dot{e}_{2i-1}\dot{\rho}_i\rho_i + e_{2i-1}\ddot{\rho}_i\rho_i - e_{2i-1}$. Combining with (12), (21), and Assumption 5, $\hat{\dot{\sigma}}_i$, $\dot{\varphi}_i$, ρ_i, $\dot{\rho}_i$, and $\dot{x}_{2i}$ can be calculated or measured, and therefore, the derivative of $\bar{\varphi}_i$ can be calculated as

$$\begin{aligned} \dot{\bar{\varphi}}_i = &-\frac{\hat{\dot{\sigma}}_i e_{2i}}{2a_1^2} - \left(\frac{\hat{\sigma}_i}{2a_1^2} + \kappa_{2i}\right)(\dot{x}_{2i} - \dot{\varphi}_i) \\ &- \frac{\left(\dot{e}_{2i-1}\rho_i^2 + e_{2i-1}^2\dot{e}_{2i-1} - 2\rho_i\dot{\rho}_i e_{2i-1}\right)}{\left(\rho_i^2 - e_{2i-1}^2\right)^2}. \end{aligned} \tag{31}$$

Remark 11. Equation (30) plays an key role for the boundedness of τ. If $\tau_i \geq \tau_{iM} - \varepsilon$, then $\dot{\tau} = [\partial \Gamma_{\tau_{iM}}(\tau_i)/\partial \tau_i]^{-1} \cdot [\omega_i - 0.5(1 + \omega_i^2)]$. Since $[\partial \Gamma_{\tau_{iM}}(\tau_i)/\partial \tau_i]^{-1} > 0$ and $\omega_i - 0.5 \cdot (1 + \omega_i^2) \leq 0$, it leads to $\dot{\tau}_i \leq 0$, and moreover, Equation (30) will

prevent τ_i from getting greater than τ_{iM}. If $\tau_i \le -\tau_{iM} + \varepsilon$, it is easy to obtain $\dot{\tau}_i \ge 0$ due to $[\partial \Gamma_{\tau_{iM}}(\tau_i)/\partial \tau_i]^{-1} > 0$ and $\varpi_i + 0.5(1+\varpi_i^2) \ge 0$. Thus, Equation (26) will prevent τ_i from getting smaller than $-\tau_{iM}$. Based on the above analysis, τ_i can be constrained within a preset interval, i.e., $\tau_i \in [-\tau_{iM}, \tau_{iM}]$.

Lemma 12. *Consider the auxiliary deviation variables s_i and $\dot{s}_i$; if the input updating laws are chosen as (30), then the following inequality can be established:*

$$s_i \cdot \dot{s}_i \le -\kappa_{2i} s_i^2 - e_{2i} s_i \quad (i = 1, 2). \tag{32}$$

Proof. The following three cases need to be discussed for the proof of Lemma 12.

Case 1. If $\tau_i \ge \tau_{iM} - \varepsilon$, from (26), we can obtain $s_i \ge 0$ and it can be verified that

$$\begin{aligned} s_i \cdot \dot{s}_i &= s_i \cdot \left(\frac{\partial \Gamma_{\tau_{iM}}(\tau_i)}{\partial \tau_i} \cdot \dot{\tau}_i - \frac{\partial \Gamma_{\bar{\varphi}_{iM}}(\bar{\varphi}_i)}{\partial \bar{\varphi}_i} \cdot \dot{\bar{\varphi}}_i \right) \\ &= s_i \cdot \left(\varpi_i - \frac{1}{2}\left(1 + \varpi_i^2\right) - \frac{\partial \Gamma_{\bar{\varphi}_{iM}}(\bar{\varphi}_i)}{\partial \bar{\varphi}_i} \cdot \dot{\bar{\varphi}}_i \right) \\ &\le -\kappa_{2i} s_i^2 - e_{2i} s_i - 0.5 \cdot s_i \cdot \left(1 + \varpi_i^2\right) \le -\kappa_{2i} s_i^2 - e_{2i} s_i. \end{aligned} \tag{33}$$

Case 2. If $|\tau_i| < \tau_{iM} - \varepsilon$, this leads to

$$s_i \cdot \dot{s}_i = s_i \left(\frac{\partial \Gamma_{\tau_{iM}}(\tau_i)}{\partial \tau_i} \dot{\tau}_i - \frac{\partial \Gamma_{\bar{\varphi}_{iM}}(\bar{\varphi}_i)}{\partial \bar{\varphi}_i} \dot{\bar{\varphi}}_i \right) \le -\kappa_{2i} s_i^2 - e_{2i} s_i. \tag{34}$$

Case 3. If $\tau_i \le -\tau_{iM} + \varepsilon$, then we have $s_i \le 0$ from (25); it yields

$$\begin{aligned} s_i \cdot \dot{s}_i &= s_i \cdot \left(\frac{\partial \Gamma_{\tau_{iM}}(\tau_i)}{\partial \tau_i} \cdot \dot{\tau}_i - \frac{\partial \Gamma_{\bar{\varphi}_{iM}}(\bar{\varphi}_i)}{\partial \bar{\varphi}_i} \cdot \dot{\bar{\varphi}}_i \right) \\ &= s_i \cdot \left(\varpi_i + \frac{1}{2}\left(1 + \varpi_i^2\right) - \frac{\partial \Gamma_{\bar{\varphi}_{iM}}(\bar{\varphi}_i)}{\partial \bar{\varphi}_i} \cdot \dot{\bar{\varphi}}_i \right) \\ &\le -\kappa_{2i} s_i^2 - e_{2i} s_i + 0.5 \cdot s_i \cdot \left(1 + \varpi_i^2\right) \le -\kappa_{2i} s_i^2 - e_{2i} s_i. \end{aligned} \tag{35}$$

From (33) to (35), Lemma 12 is proven. □

Now, the main results are summarized as follows.

Theorem 13. *Consider the dynamics system (10) with Assumptions 2-4, if the virtual control laws (16) and (20) with parameter updating law as specified in Equations (21) are used and the input updating laws (30) are implemented, then for any initial states in Ω, the following control objectives can be achieved.*

(1) All signals in the closed-loop system are semiglobal uniformly ultimately bounded

(2) The fixed-time prescribed performance is achieved, such that the tracking errors $e_{2i-1}(i = 1, 2)$ converge to a prescribed compact set $\Omega_e = \{e_{2i-1}, ||e_{2i-1}| < \rho_{TS}\}$ for $\forall t > T_S$

Proof. Choose the Lyapunov function candidate V as

$$V = \frac{1}{2} \cdot \sum_{i=1}^{2} \left(\log \frac{\rho_i^2}{\rho_i^2 - e_{2i-1}^2} + e_{2i}^2 + s_i^2 \right) + \frac{1}{2} \cdot \sum_{i=1}^{2} \frac{\tilde{\sigma}_i^2}{\xi_i}, \tag{36}$$

where $\tilde{\sigma}_i = \sigma_i - \hat{\sigma}_i$. The time derivative of V is expressed as

$$\begin{aligned} \dot{V} &= \sum_{i=1}^{2} \left(\frac{1}{2} \frac{\rho_i^2 - e_{2i-1}^2}{\rho_i^2} \cdot \frac{2\rho_i \dot{\rho}_i \left(\rho_i^2 - e_{2i-1}^2\right) - \rho_i^2 \left(2\rho_i \dot{\rho}_i - 2e_{2i-1}\dot{e}_{2i-1}\right)}{\left(\rho_i^2 - e_{2i-1}^2\right)^2} \right) \\ &\quad + \sum_{i=1}^{2} \left(e_{2i} \cdot \dot{e}_{2i} + s_i \cdot \dot{s}_i\right) - \sum_{i=1}^{2} \frac{\tilde{\sigma}_i \dot{\hat{\sigma}}_i}{\xi} \\ &= \sum_{i=1}^{2} \left(\frac{e_{2i-1}\dot{e}_{2i-1}}{\rho_i^2 - e_{2i-1}^2} - \frac{\dot{\rho}_i e_{2i-1}^2}{\rho_i \left(\rho_i^2 - e_{2i-1}^2\right)} + e_{2i}\dot{e}_{2i} + s_i \dot{s}_i \right) \\ &\quad - \sum_{i=1}^{2} \left(\frac{e_{2i}^2 \tilde{\sigma}_i}{2a_1^2} - a_1 \tilde{\sigma}_i \hat{\sigma}_i \right). \end{aligned} \tag{37}$$

□

Based on (17), (27), and (29), the following relationships are established in the compact set Ω:

$$\begin{cases} (1)\ e_{2i-1}\dot{e}_{2i-1} = e_{2i-1}e_{2i} - \kappa_{2i-1} \cdot e_{2i-1}^2 + \dfrac{e_{2i-1}^2 \dot{\rho}_i}{\rho_i}, \\ (2) e_{2i}\Psi_i \le \dfrac{\sigma_i e_{2i}^2}{2a_1^2} + \dfrac{a_1^2}{2}, \\ (3)\ e_{2i}\dot{e}_{2i} \le e_{2i}s_i - \kappa_{2i}e_{2i}^2 - \dfrac{e_{2i-1}e_{2i}}{\rho_i^2 - e_{2i-1}^2} + \dfrac{\tilde{\sigma}_i e_{2i}^2}{2a_1^2} + \dfrac{a_1^2}{2}, \\ (4)\ \dfrac{e_{2i-1}^2}{\rho_i^2 - e_{2i-1}^2} \ge \log \dfrac{\rho_i^2}{\rho_i^2 - e_{2i-1}^2}, \\ (5)\ a_1 \tilde{\sigma}_i \hat{\sigma}_i \le -\dfrac{a_1 \xi_i \tilde{\sigma}_i^2}{2\xi_i} + \dfrac{a_1 \sigma_i^2}{2}. \end{cases} \tag{38}$$

With the help of (38), then (37) becomes

$$\begin{aligned} \dot{V} &\le \sum_{i=1}^{2} \left(-\kappa_{2i-1} \log \frac{\rho_i^2}{\rho_i^2 - e_{2i-1}^2} - \kappa_{2i} e_{2i}^2 - \kappa_{2i} s_i^2 + \frac{\tilde{\sigma}_i e_{2i}^2}{2a_1^2} \right) \\ &\quad + \sum_{i=1}^{2} \left(-\frac{\tilde{\sigma}_i e_{2i}^2}{2a_1^2} + a_1 \tilde{\sigma}_i \hat{\sigma}_i \right) + a_1^2 \\ &\le \sum_{i=1}^{2} \left(-\kappa_{2i-1} \log \frac{\rho_i^2}{\rho_i^2 - e_{2i-1}^2} - \kappa_{2i} e_{2i}^2 - \kappa_{2i} s_i^2 - \frac{a_1 \xi_i \tilde{\sigma}_i^2}{2\xi_i} \right) \\ &\quad + \sum_{i=1}^{2} \frac{a_1 \sigma_i^2}{2} + a_1^2 \le -\alpha_g \cdot V + \Delta_g, \end{aligned} \tag{39}$$

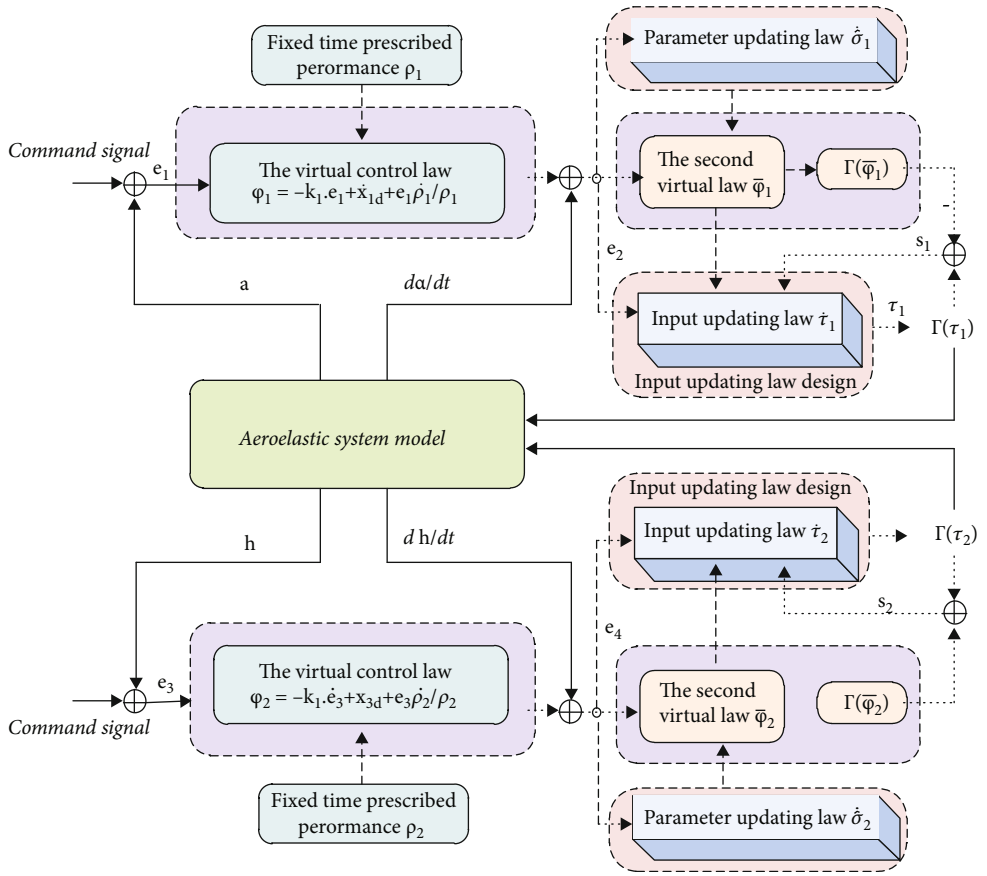

Figure 4: The closed-loop system structure.

where $\alpha_g = \min\{\kappa_{2i}, \kappa_{2i-1}, a_1\xi_i\}$ and $\Delta_g = (a_1^2/2) + \sum_{i=1}^{2}(a_1\sigma_i^2/2)$. Solving (39), we have

$$0 \le V(t) \le \frac{\Delta_g}{\alpha_g} + \left(V(0) - \frac{\Delta_g}{\alpha_g}\right) \cdot e^{-\alpha_g t}. \tag{40}$$

According to (40), it can be seen that each signal of the closed-loop system is bounded, and meanwhile, we can obtain that

$$\frac{1}{2}\log\frac{\rho_i^2}{\rho_i^2 - e_{2i-1}^2} \le \frac{\Delta_g}{\alpha_g} + V(0). \tag{41}$$

Taking exponentials on both sides of (41) yields

$$e_{2i-1}^2 \le \rho_i^2\left(1 - e^{-2\left(\Delta_g/\alpha_g + V(0)\right)}\right) < \rho_i^2. \tag{42}$$

Therefore, in the light of the properties of $\rho_i(t)$, we obtain $|e_{2i-1}| < \rho_i(t)$; it implies $e_{2i-1}(t) < \rho_{TS}$ for $t \in [T_S, \infty)$. Then, one can conclude that tracking control with the fixed-time prescribed performance is achieved. The control system structure and algorithm flow chart are shown in Figures 4 and 5, respectively.

From the above analysis, e_{2i-1} remain bounded inside the region $B_e \triangleq \{|e_{2i-1}| < \rho_i(t),\ i = 1, 2\}$ for $t \ge T_S$. It should be pointed that the reciprocal of $\partial\Gamma_{\tau_{iM}}(\tau_i)/\partial\tau_i$ plays an important role in the designed input updating law (30). In fact, the input updating law singularity may occur since $\partial\Gamma_{\tau_{iM}}(\tau_i)/\partial\tau_i$ goes to zero as $\tau_i \longrightarrow \infty$. However, from (30), we can see that variable τ_i remains bounded inside the region $B_\tau \triangleq \{|\tau_i| \le \tau_{iM},\ i = 1, 2\}$ for $t \ge 0$. Hence, the sensibility of the reciprocal of $\partial\Gamma_{\tau_{iM}}(\tau_i)/\partial\tau_i$ can be acceptable, and moreover, $\partial\Gamma_{\tau_{iM}}(\tau_i)/\partial\tau_i$ has never gone to zero.

Remark 14. To ensure that $\rho_i^2(0) > e_{2i-1}^2(0)$ $(i = 1, 2)$, the design parameter ρ_0 (ρ_0 is given in (12)) needs to satisfy $\rho_0 > e_{2i-1}(0)$. Combining with (40) and (41), we can obtain that $|e_{2i-1}| < \rho_i(t)$ for $\forall t \in [0,\infty)$; it is obvious that the system error constraints are not violated; namely, $|e_{2i-1}|$ are always less than the fixed-time performance function.

Remark 15. The designed method is a recursive design process borrowed from the traditional backstepping control design idea. Because τ_i are contained within the function $\Gamma_{\tau_{iM}}(\tau_i)$, therefore, we cannot design the control laws τ_i in the form of the function $\Gamma_{\tau_{iM}}(\tau_i)$. To solve this problem and complete the control law design, $s_i(i = 1, 2)$ are introduced such that input updating laws $\dot{\tau}_i$ can be designed by taking the derivative of s_i. On the other hand, from (26), $s_i(i = 1, 2)$ have a "supervisory role" when τ_i exceeding

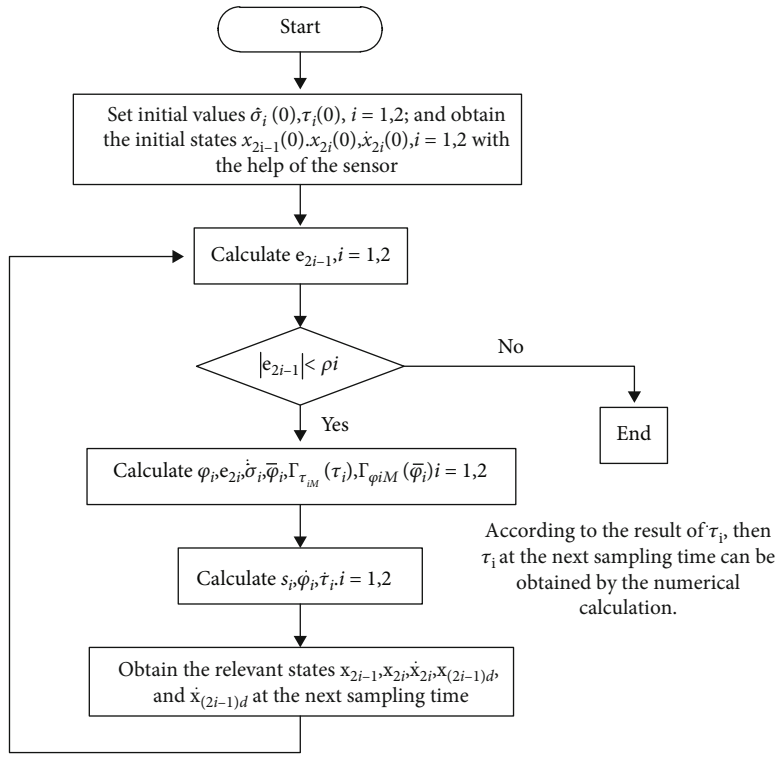

Figure 5: The algorithm flow chart.

Table 3: The control parameter configuration.

Control method	
PPAC	$\kappa_{2i-1} = \kappa_{2i} = 3, a_1 = \varepsilon = 0.1, c = \rho_0 = 0.5, \xi_i = 10, \rho_{TS} = 8 \times 10^{-5}, T_s = 2, \tau_{iM} = 8$
ASMC	$k_1 = k_2 = 5, p_1 = p_2 = 1, l_1 = l_2 = 1, \varepsilon_c = 0.03, \varphi = 2.5, \eta = 7$

the setting values (i.e., $s_i \geq 0$ if $\tau_i \geq \tau_{iM} - \varepsilon$; $s_i \leq 0$ if $\tau_i \leq -\tau_{iM} + \varepsilon$). With the help of (33)-(35), we have $s_i \cdot \dot{s}_i \leq -\kappa_{2i} s_i^2 - e_{2i} s_i$, which can help us get the inequality result $\dot{V} \leq -\alpha_g V + \Delta_g$ and obtain the stability result of the closed-loop system on this basis.

Remark 16. The tuning guidelines for all the designed parameters are summarized as follows:

(1) From (39), larger κ_{2i}, κ_{2i-1}, ξ_i, and $1/a_1 (i = 1, 2)$ result in smaller system errors (e_{2i} and s_i) but may lead to the large control magnitude and excite the undesired high-frequency dynamics of the controlled system. In this paper, these parameters are set to small positive numbers, and our concern is to adjust them to establish the bound of system error e_{2i-1}. Therefore, the process of choosing the control parameters κ_{2i}, κ_{2i-1}, ζ_i, and $1/a_1$ is significantly simplified

(2) The prescribed performance parameter ρ_0 should be chosen large enough such that the initial error boundedness can be satisfied, i.e., $\max\{|\alpha^{\max} - x_{1d}(0)|, |h^{\max} - x_{3d}(0)|\} < \rho_0$. The parameter ρ_{TS} determines the final bound of the steady-state error. The parameter T_S determines the time for the tracking error to converge to the specified accuracy. Too small T_S can lead to a large control amplitude at the beginning of the control. Combined with the actual control tasks, moderate compromise selection of T_S and ρ_{TS} can eliminate the large amplitude for control output at the beginning of the control process

Remark 17. The prescribed performance control methods [23–26] can ensure that the designed closed-loop system has good transient and steady-state behaviors and forces the tracking error to converge to a predetermined range when the time tends to infinity. It is worth mentioning that the above-mentioned methods are developed based on traditional performance functions, which means that the designed control systems by these methods are not equipped with the finite-time prescribed performance. Although some new

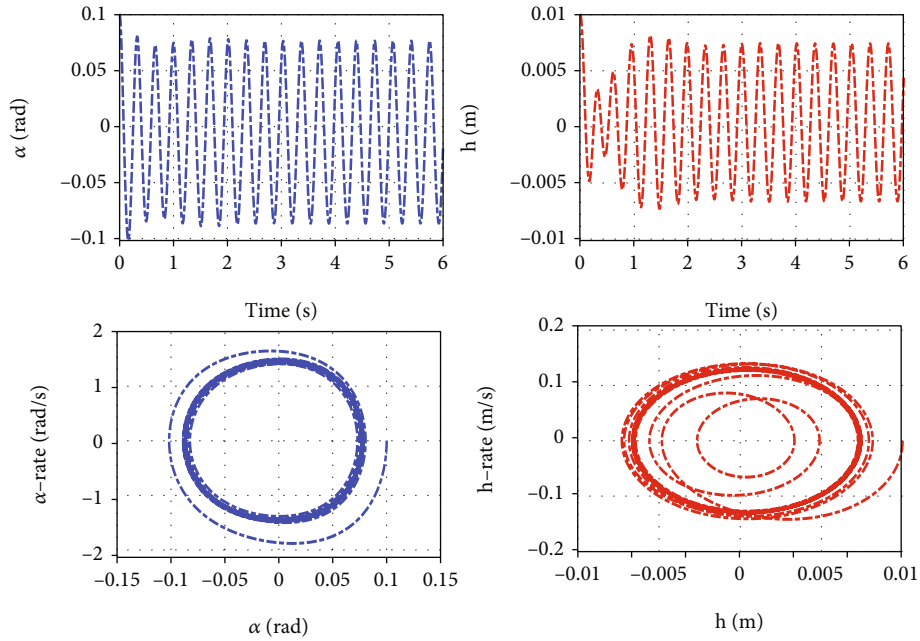

Figure 6: The open-loop responses of the aeroelastic system.

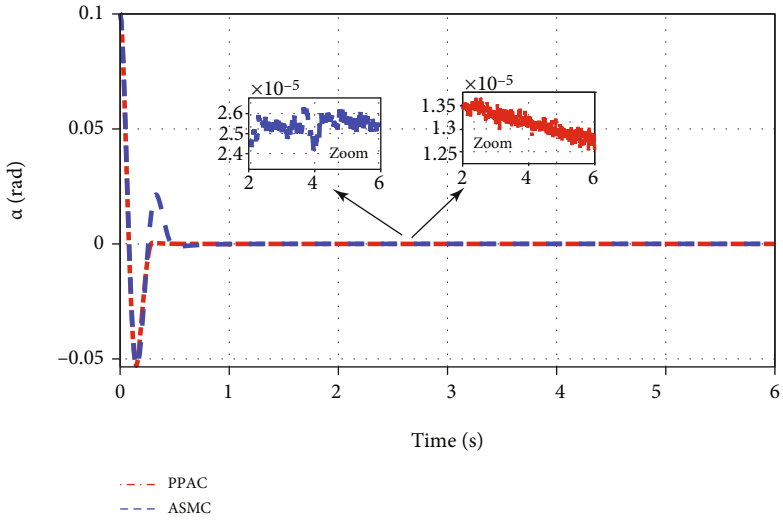

Figure 7: α responses of the closed-loop system with Case 1.

nonlinear control approaches are proposed in [45, 46] to achieve finite-time prescribed performance tracking control, the settling time is related to the initial value of the system states. In this paper, the proposed settling time T_S is independent of the initial conditions, and therefore, T_S can be set according to the requirement of control tasks.

4. Numerical Simulations

In this section, simulation results are presented to illustrate the effectiveness of our proposed control method. The system parameters satisfy $y = \bar{y} + \Delta y$ in which $\bar{y}$ and Δy represent the nominal part and uncertain part, respectively. The nominal part of system parameters are chosen from experimental date in [4, 47]. The initial value of system states are given as $\alpha(0) = 0.1$ rad, $h(0) = 0.01\,m$, and $\dot{\alpha}(0) = \dot{h}(0) = \ddot{\alpha}(0) = \ddot{h}(0) = 0$. Since the control objective is to suppress the aeroelastic vibrations, thus the desired signals are set as zero.

To evaluate the performance of the proposed control method, a comparison will be given between the prescribed performance adaptive compensation control scheme (PPAC)

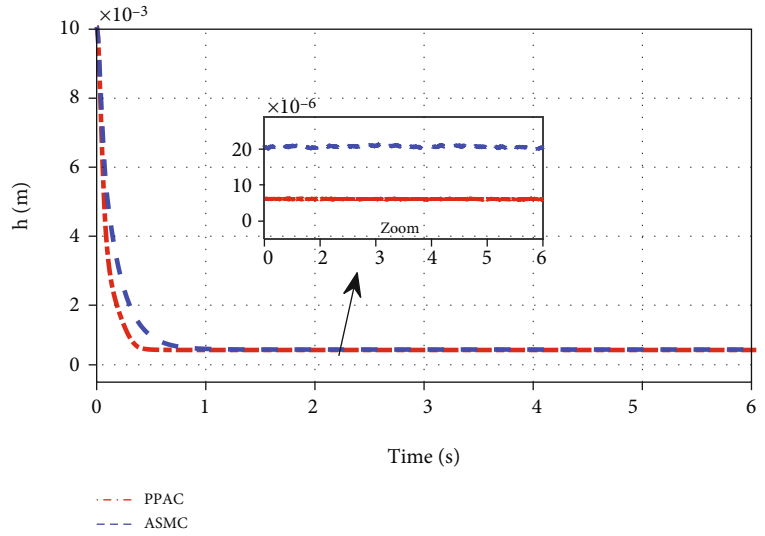

Figure 8: h responses of the closed-loop system with Case 1.

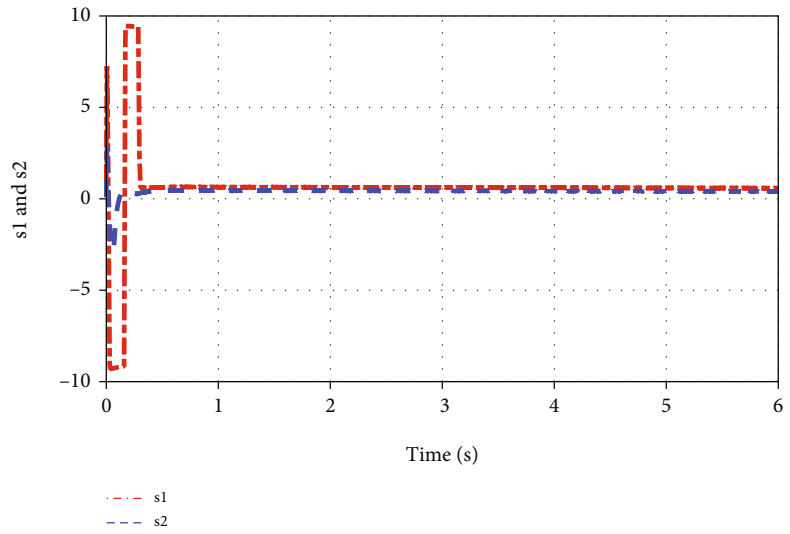

Figure 9: s_1 and s_2 responses with Case 1.

proposed in this paper and the adaptive sliding mode compensation control scheme (ASMC) in [5] for the same sampling time and model parameters. The control system parameters of PPAC and ASMC are set in Table 3. According to [5], the ASMC controller is devised as

$$u_{\mathrm{ASMC}} = -f_n - ks_1 - \int_0^t \left[\eta \,\mathrm{sign}\,(\sigma) + k_2(s_1 + s_2) + \frac{\varphi^2\sigma}{4} + l\widehat{\alpha}^2 + \frac{\widehat{\alpha}}{4\varphi\sigma}\right] d\tau, \tag{43}$$

where f_n is a known function consisting of the system nominal parameter; s_1 and s_2 are the system error vectors; k_1, k_2, η, and φ are design parameters; $\sigma = [\sigma_1, \sigma_2]^T = s_2 + k \times s_1 + p \times \int_o^t s_1 d\tau$ ($k = \mathrm{diag}\,\{k_1, k_2\} > 0$, $l = \mathrm{diag}\,\{l_1, l_2\} > 0$, and $p = \mathrm{diag}\,\{p_1, p_2\} > 0$); and $\widehat{\alpha} = \mathrm{diag}\,\{\widehat{\alpha}_1, \widehat{\alpha}_2\}$ is the disturbance estimation.

Firstly, the open-loop responses for sinusoidal gust $w_G = 0.07$ and $U = 13.28 m/s$ are shown in Figure 6; in this situation, the system exhibited the limit cycle oscillation. It is obvious that the plunge and pitch motions represent flutter phenomena, which need to be suppressed.

For the purpose of examining the robustness of the proposed control scheme, the following two cases are executed by choosing different disturbances and unknown parameter parts.

Case A. It is assumed that $U = 13.28$ m/s, $w_G = (1 - e^{-0.25Ut/b})$, and $\Delta y = 25\% \times \mathrm{rand}\,(t) \times \bar{y}$ (note that rand (t) can generate random numbers in the interval $(0, 1)$ by using

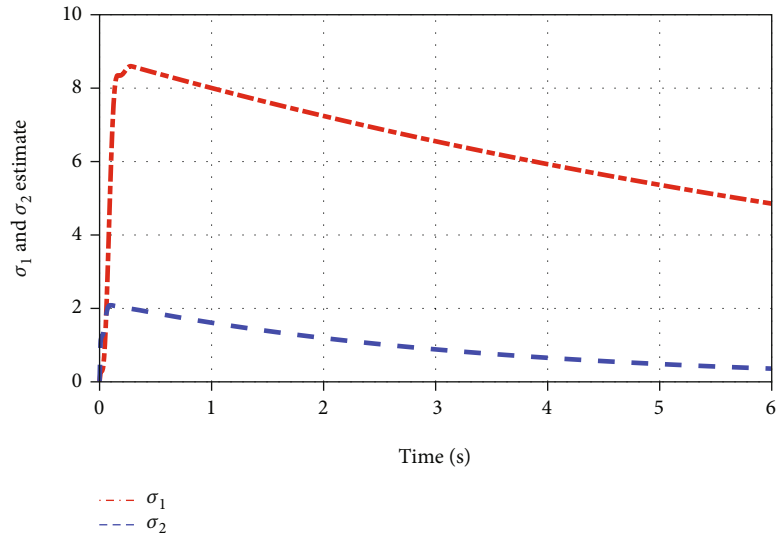

FIGURE 10: $\widehat{\sigma}_1$ and $\widehat{\sigma}_2$ responses with Case 1.

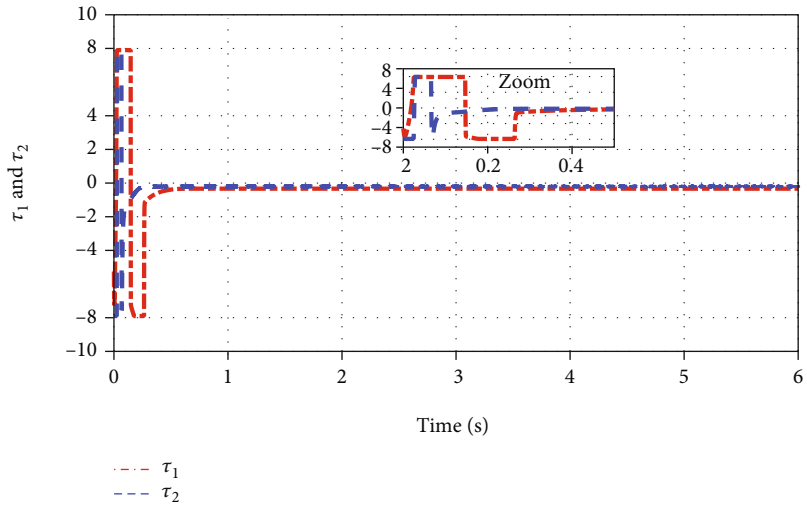

FIGURE 11: Control input of the proposed method with Case 1.

Matlab/Simulink). Figures 7–9 show the control effect under the two control methods. Compared with ASMC, the proposed method has a fast convergence rate at the initial stage, and moreover, the proposed method guarantees that the system error converges into a bounded region when $t > 2s$, i.e., $\max\{|e_1|, |e_3|\} < 8 \times 10^{-5}$. Obviously, the simulation results are perfectly matched with Theorem 13. The proposed method realizes the preset control precision after a specified time (as stated by Theorem 13, e_{2i-1} converge to a prescribed compact set $\Omega_e = \{e_{2i-1} \mid |e_{2i-1}| < \rho_{TS},\}$ for $\forall t > T_S$ based on $\rho_{TS} = 8 \times 10^{-5}$ and $T_S = 2s$). It means that the proposed control strategy is an effective way to suppress the limit cycle oscillation feature even in the presence of parameter uncertainties. As for ASMC, the maximum errors are shown as $\max\{|e_1|, |e_3|\} < 5.8 \times 10^{-4}$. From Figures 10 and 11, it can be seen that the initial amplitude values of control input τ_i and nonlinear function estimation $\widehat{\sigma}_i$ are large. This is because the proposed method is tuning and does not adapt to the adverse factors at the beginning. And then, the adaptation updating algorithm starts to exert its effectiveness such that the satisfactory control performance is achieved.

Case B. $U = 13.28$ m/s, $w_G = 2.5 \cdot (1 - e^{-0.25Ut/b}) \cdot \text{rand}(t)$, and $\Delta y = 40\% \times \text{rand}(t) \times \bar{y}$. From Figures 12–16, we see that the proposed method can guarantee that $e_{2i-1}(i = 1, 2)$ converge into a bounded region $\max\{|e_1|, |e_3|\} < 8 \times 10^{-5}$ for $t > 2s$, but the errors obtained by ASMC stay in $\max\{|e_1|, |e_3|\} < 1.8 \times 10^{-3}$ for $t > 2s$. Obviously, the

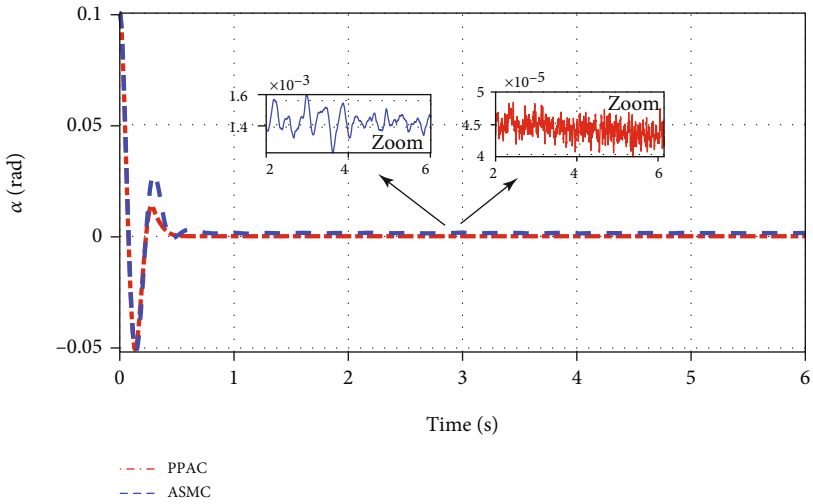

Figure 12: α responses of the closed-loop system with Case 2.

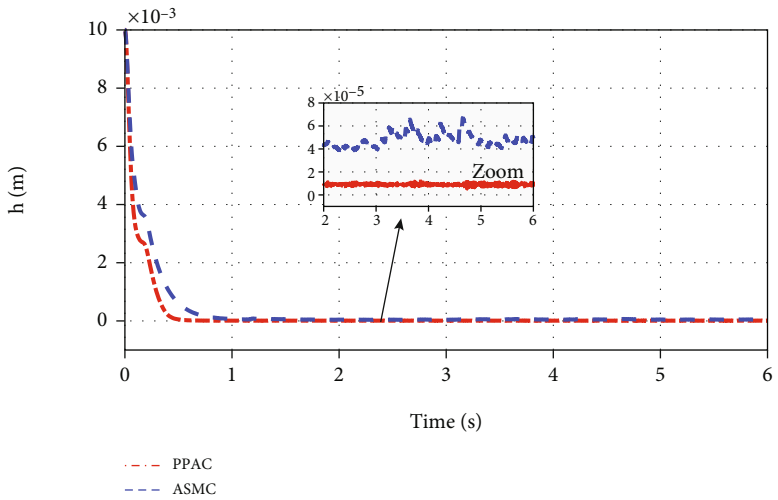

Figure 13: h responses of the closed-loop system with Case 2.

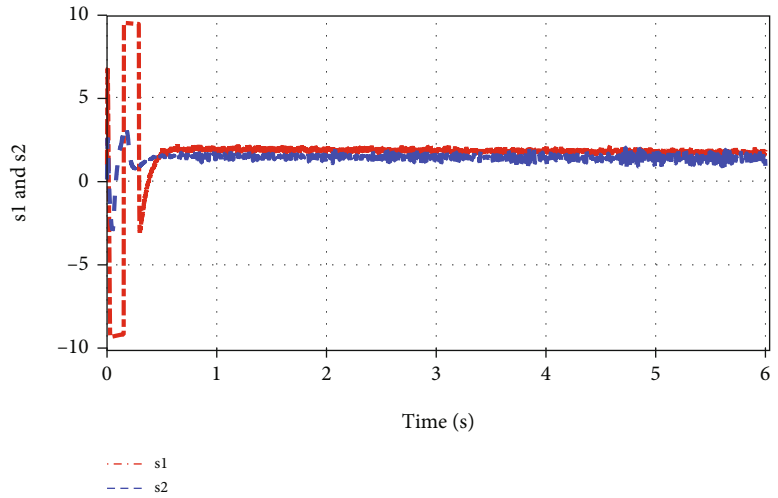

Figure 14: s_1 and s_2 responses with Case 2.

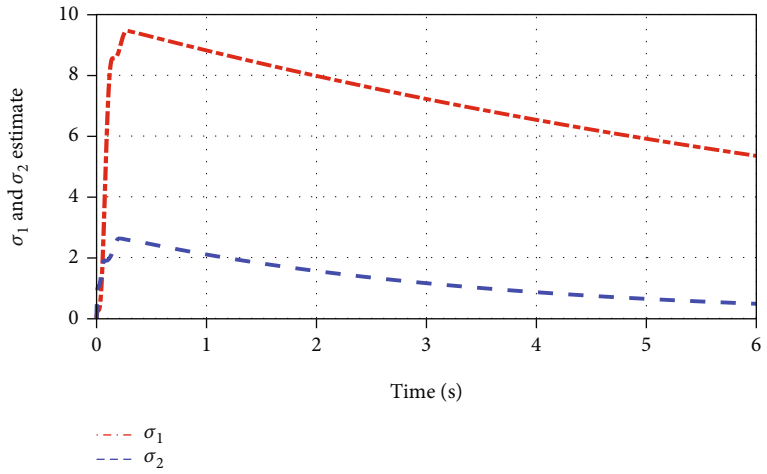

FIGURE 15: $\widehat{\sigma}_1$ and $\widehat{\sigma}_2$ responses with Case 2.

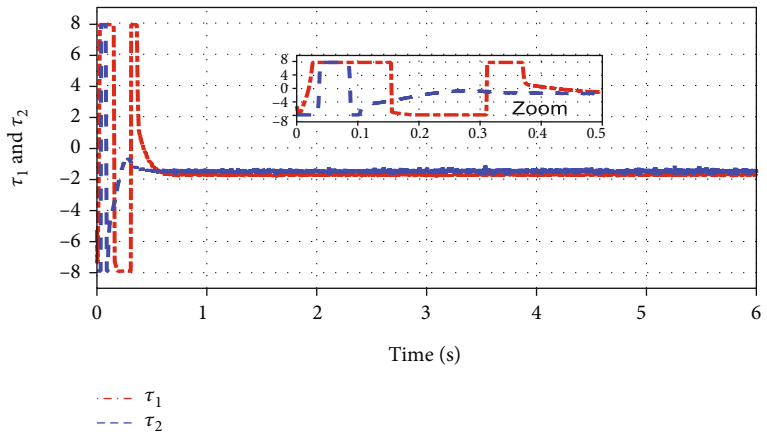

FIGURE 16: Control input of the proposed method with Case 2.

simulation results indicate that the control accuracy of the proposed method is still higher than that of ASMC. Compared with Case A, although uncertainties and the disturbance are increased, the proposed control method still achieves the fixed-time prescribed performance, and it means that the system parameter uncertainties and external disturbances are well suppressed. These simulation results show that the good performance can be obtained by the proposed control algorithm.

5. Conclusion

In this paper, a fixed-time prescribed performance control algorithm for a nonlinear aeroelastic system is presented. In particular, the control performance of the closed-loop system is guaranteed theoretically with prescribed performance constraint and excellent disturbance rejection capability. The performance of the proposed control system is evaluated by digital simulation in the presence of input constraints. Simulation results show that the designed control method suppresses the limit-cycle oscillations, despite parameter uncertainties and wind gust.

Appendix

A. Proof of the Three Properties of Lemma 1

(1) According to (8), one has

$$\frac{\partial \Gamma_{\tau_{iM}}(\tau_i)}{\partial \tau_i} = \frac{e^{2c\tau_{iM}} - e^{-2c\tau_{iM}}}{\left(e^{c\tau_{iM}} e^{c\tau_i} + e^{-c\tau_{iM}} e^{-c\tau_i}\right)\left(e^{-c\tau_{iM}} e^{c\tau_i} + e^{c\tau_{iM}} e^{-c\tau_i}\right)} > 0 \tag{A.1}$$

(2) Based on (8), we obtain $\Delta\tau_i = u_i - \Gamma_{\tau_{iM}}(\tau_i)$; therefore, $\Delta\tau_i$ satisfies

$$\begin{cases} 0 < \Delta\tau_i \le \tau_{iM} - \dfrac{1}{2c}\ln\left(\dfrac{e^{2c\tau_{iM}} + e^{-2c\tau_{iM}}}{2}\right), & \text{if } \tau_i \ge \tau_{iM}, \\ |\Delta\tau_i| \le \tau_{iM} - \dfrac{1}{2c}\ln\left(\dfrac{e^{2c\tau_{iM}} + e^{-2c\tau_{iM}}}{2}\right), & \text{if } |\tau_i| < \tau_{iM}, \\ -\tau_{iM} + \dfrac{1}{2c}\ln\left(\dfrac{e^{2c\tau_{iM}} + e^{-2c\tau_{iM}}}{2}\right) \le \Delta\tau_i \le 0, & \text{if } \tau_i \le -\tau_{iM} \end{cases} \tag{A.2}$$

In the light of (A.2), then

$$|\Delta\tau_i| \le \tau_{iM} - \frac{1}{2c}\ln\left(\frac{e^{2c\tau_{iM}} + e^{-2c\tau_{iM}}}{2}\right). \tag{A.3}$$

Hence, $\lim_{c\longrightarrow+\infty} \Delta\tau_i = 0$.

(3) Due to $\Gamma_{\tau_{iM}}(\tau_i) = (1/2c)\ln\left(\left(e^{c\tau_{iM}}e^{c\tau_i} + e^{-c\tau_{iM}}e^{-c\tau_i}\right)/\left(e^{-c\tau_{iM}}e^{c\tau_i} + e^{c\tau_{iM}}e^{-c\tau_i}\right)\right)$, we have

$$\begin{cases} \lim\limits_{\tau_i\longrightarrow+\infty}\Gamma_{\tau_{iM}}(\tau_i) = \lim\limits_{\tau_i\longrightarrow+\infty}\left[\dfrac{1}{2c}\cdot\ln\left(\dfrac{e^{2c\tau_{iM}} + e^{-2c\tau_i}}{1 + e^{c\tau_{iM}}e^{-2c\tau_i}}\right)\right] = \dfrac{2c\tau_{iM}}{2c} = \tau_{iM}, \\ \lim\limits_{\tau_i\longrightarrow-\infty}\Gamma_{\tau_{iM}}(\tau_i) = \lim\limits_{\tau_i\longrightarrow-\infty}\left[\dfrac{1}{2c}\cdot\ln\left(\dfrac{e^{2c\tau_i} + e^{-2c\tau_{iM}}}{1 + e^{-2c\tau_{iM}}e^{2c\tau_i}}\right)\right] = \dfrac{-2c\tau_{iM}}{2c} = -\tau_{iM}. \end{cases} \tag{A.4}$$

According to (A.4), we can conclude that $|\Gamma_{\tau_{iM}}(\tau_i)| \le \tau_{iM}$.

Data Availability

The data used to support the findings of this study are included within the article.

Conflicts of Interest

The authors declare that they have no conflicts of interest.

Acknowledgments

This work is supported in part by the Liaoning Provincial Department of Education Project under Grant J2020112 and the Natural Science Foundation of Liaoning Province (China) under Grant 2019-ZD-0131.

References

[1] Y. Bichiou, M. R. Hajj, and A. H. Nayfeh, "Effectiveness of a nonlinear energy sink in the control of an aeroelastic system," *Nonlinear Dynamic*, vol. 86, no. 4, pp. 2161–2177, 2016.

[2] H. H. Dai, X. K. Yue, and D. Xie, "Chaos and chaotic transients in an aeroelastic system," *Journal of Sound and Vibration*, vol. 26, pp. 7267–7285, 2014.

[3] L. Q. Dou, R. Ji, and J. Q. Gao, "Identification of nonlinear aeroelastic system using fuzzy wavelet neural network," *Neurocomputing*, vol. 214, pp. 935–943, 2016.

[4] D. C. Li, J. W. Xiang, and S. J. Guo, "Adaptive control of a nonlinear aeroelastic system," *Aerospace Science and Technology*, vol. 12, pp. 343–352, 2011.

[5] Z. K. Song and H. X. Li, "Second-order sliding mode control with backstepping for aeroelastic systems based on finite-time technique," *International Journal of Control Automation and Systems*, vol. 11, no. 2, pp. 416–421, 2013.

[6] W. H. Su and W. Song, "A real-time hybrid aeroelastic simulation platform for flexible wings," *Aerospace Science and Technology*, vol. 95, pp. 105–113, 2019.

[7] J. S. Song, J. Choo, S. J. Cha, and S. Na, "Robust aeroelastic instability suppression of an advanced wing with model uncertainty in subsonic compressible flow field," *Aerospace Science and Technology*, vol. 20, pp. 435–446, 2012.

[8] H. W. Yun and J. L. Han, "Robust flutter analysis of a nonlinear aeroelastic system with parametric uncertainties," *Aerospace Science and Technology*, vol. 13, no. 2-3, pp. 139–149, 2009.

[9] J. Ko, T. W. Strganac, and A. J. Kurdila, "Stability and control of a structurally nonlinear aeroelastic system," *Journal of Guidance Control and Dynamics*, vol. 21, no. 5, pp. 718–725, 1998.

[10] C. L. Chen, C. C. Peng, and H. T. Yau, "High-order sliding mode controller with backstepping design for aeroelastic systems," *Communications in Nonlinear Science and Numerical Simulation*, vol. 17, no. 4, pp. 1813–1823, 2012.

[11] S. N. Singh and W. Yim, "State feedback control of an aeroelastic system with structural nonlinearity," *Aerospace Science and Technology*, vol. 7, no. 1, pp. 23–31, 2003.

[12] M. Tadi, "State-dependent Riccati equation for control of aeroelastic flutter," *Journal of Guidance, Control, and Dynamics*, vol. 26, no. 6, pp. 914–917, 2003.

[13] N. Bhoir and S. N. Singh, "Control of unsteady aeroelastic system via state-dependent Riccati equation method," *Journal of Guidance, Control, and Dynamics*, vol. 28, no. 1, pp. 78–84, 2005.

[14] D. Li, S. Guo, and J. Xiang, "Aeroelastic dynamic response and control of an airfoil section with control surface nonlinearities," *Journal of Sound and Vibration*, vol. 329, no. 22, pp. 4756–4771, 2010.

[15] C. C. Marsden and S. J. Price, "Transient and limit cycle simulation of a nonlinear aeroelastic system," *Journal of Aircraft*, vol. 44, no. 1, pp. 60–70, 2007.

[16] C. M. Lin and W. L. Chin, "Adaptive decoupled fuzzy sliding-mode control of a nonlinear aeroelastic system," *Journal of Guidance, Control, and Dynamics*, vol. 29, no. 1, pp. 206–209, 2006.

[17] Z. Wang, A. Behal, and P. Marzocca, "Model-free control design for multi-input multi-output aeroelastic system subject to external disturbance," *Journal of Guidance, Control, and Dynamics*, vol. 34, no. 2, pp. 446–458, 2011.

[18] K. W. Lee and S. N. Singh, "Adaptive control of multi-input aeroelastic system with constrained inputs," *Journal of Guidance, Control, and Dynamics*, vol. 38, no. 12, pp. 2337–2350, 2015.

[19] K. W. Lee and S. N. Singh, "Robust finite-time continuous control of an unsteady aeroelastic system," *Journal of Guidance, Control, and Dynamics*, vol. 41, no. 4, pp. 978–986, 2018.

[20] J. X. Yuan, N. Qi, Z. Qiu, and F. X. Wang, "Adaptive RBF observer-sliding mode controller design for a two dimensional aeroelastic system with unsteady aerodynamics," *Aerospace Science and Technology*, vol. 80, pp. 482–495, 2018.

[21] M. Z. Majid, "Adaptive interval type-2 fuzzy recurrent RBFNN control design using ellipsoidal membership functions with

application to MEMS gyroscope," *ISA Transactions*, vol. 119, pp. 25–40, 2022.

[22] R. H. Vafaie, A. Mohammadzadeh, and M. Piran, "A new type-3 fuzzy predictive controller for MEMS gyroscopes," *Nonlinear Dynamics*, vol. 106, pp. 381–403, 2021.

[23] C. P. Bechlioulis and G. A. Rovithakis, "Adaptive control with guaranteed transient and steady state tracking error bounds for strict feedback systems," *Automatica*, vol. 45, no. 2, pp. 532–538, 2009.

[24] J. Na, Q. Chen, X. Ren, and Y. Guo, "Adaptive prescribed performance motion control of servo mechanisms with friction compensation," *IEEE Transactions on Industrial Electronics*, vol. 61, no. 1, pp. 486–494, 2014.

[25] W. Wang and C. Wen, "Adaptive actuator failure compensation control of uncertain nonlinear systems with guaranteed transient performance," *Automatica*, vol. 46, no. 12, pp. 2082–2091, 2010.

[26] C. P. Benchlioulis and G. A. Rovithakis, "Robust partial-state feedback prescribed performance control of cascade systems with unknown nonlinearities," *IEEE Transactions on Automatic Control*, vol. 56, no. 9, pp. 2224–2230, 2011.

[27] Q. L. Hu, X. D. Shao, and L. Guo, "Adaptive fault-tolerant attitude tracking control of spacecraft with prescribed performance," *IEEE Transactions on Mechatronics*, vol. 23, no. 1, pp. 331–341, 2018.

[28] Z. K. Song and K. B. Sun, "Adaptive compensation control for attitude adjustment of quadrotor unmanned aerial vehicle," *ISA Transacions*, vol. 69, pp. 242–255, 2017.

[29] Z. K. Song, S. Ling, and K. Sun, "Adaptive fault tolerant attitude tracking control for miniature rotorcrafts under actuator saturation," *Aerospace Science and Technology*, vol. 69, pp. 27–38, 2017.

[30] C. C. Hua, G. P. Liu, L. Li, and X. P. Guan, "Adaptive fuzzy prescribed performance control for nonlinear switched time-delay systems with unmodeled dynamics," *IEEE Transactions on Fuzzy Systems*, vol. 26, no. 4, pp. 1934–1945, 2018.

[31] X. L. Shao, H. N. Si, and W. D. Zhang, "Fuzzy wavelet neural control with improved prescribed performance for MEMS gyroscope subject to input quantization," *Fuzzy Sets and Systems*, vol. 411, pp. 136–154, 2021.

[32] C. Zhu, J. F. Zeng, B. Huang, Y. M. Su, and Z. Y. Su, "Saturated approximation-free prescribed performance trajectory tracking control for autonomous marine surface vehicle," *Ocean Engineering*, vol. 237, pp. 1–15, 2021.

[33] Y. Q. Wang, Y. Chang, F. A. Abdulhameed, and D. A. Naif, "Adaptive fuzzy output-feedback tracking control for switched nonstrict-feedback nonlinear systems with prescribed performance," *Circuits, Systems, and Signal Processing*, vol. 40, no. 1, pp. 88–113, 2021.

[34] W. He, Y. Dong, and C. Sun, "Adaptive neural impedance control of a robotic manipulator with input saturation," *IEEE Transactions on Systems, Man, and Cybernetics: Systems*, vol. 46, no. 3, pp. 334–344, 2016.

[35] X. Yan, M. Chen, G. Feng, Q. Wu, and S. Shao, "Fuzzy robust constrained control for nonlinear systems with input saturation and external disturbances," *IEEE Transactions on Fuzzy Systems*, vol. 29, no. 2, pp. 345–356, 2021.

[36] Q. Zhou, P. Shi, Y. Tian, and M. Wang, "Approximation-based adaptive tracking control for MIMO nonlinear systems with input saturation," *IEEE Transactions on Cybernetics*, vol. 45, no. 10, pp. 2119–2128, 2015.

[37] Y. Y. Gao, H. B. Li, X. M. Dong, and Z. C. Liu, "Constrained adaptive neural network control of an MIMO aeroelastic system with input nonlinearities," *Chinese Journal of Aeronautics*, vol. 30, pp. 796–806, 2017.

[38] X. Z. Xu, W. X. Wu, and W. G. Zhang, "Sliding mode control for a nonlinear aeroelastic system through backstepping," *Journal Aerospace Engineering*, vol. 31, pp. 451–462, 2018.

[39] X. Gang, Y. Xia, D. Zhai, and D. Ma, "Adaptive prescribed performance terminal sliding mode attitude control for quadrotor under input saturation," *IET Control Theory and Applications*, vol. 14, pp. 2473–2480, 2020.

[40] Y. Hao, Z. Lin, Z. Su, Y. Xiao, and B. Huang, "Robust adaptive control for spacecraft rendezvous with predefined-time prescribed performance and input saturation," *Journal of Aerospace Engineering*, vol. 35, 2022.

[41] Z. K. Song and K. B. Sun, "Adaptive fault tolerant control for a small coaxial rotor unmanned aerial vehicles with partial loss of actuator effectiveness," *Aerospace Science and Technology*, vol. 88, pp. 362–379, 2019.

[42] Z. K. Song and K. B. Sun, "Prescribed performance adaptive control for an uncertain robotic manipulator with input compensation updating law," *Journal of the Franklin Institute*, vol. 358, no. 16, pp. 8396–8418, 2021.

[43] Z. K. Song and K. B. Sun, "Prescribed performance tracking control for a class of nonlinear system considering input and state constraints," *ISA Transactions*, vol. 119, pp. 81–92, 2022.

[44] J. W. Tao, T. Zhang, and Q. Liu, "Novel finite-time adaptive neural control of flexible spacecraft with actuator constraints and prescribed attitude tracking performance," *Acta Astronautica*, vol. 179, pp. 646–658, 2021.

[45] W. Sun, Y.-Q. Wu, and Z.-Y. Sun, "Command filter-based finite-time adaptive fuzzy control for uncertain nonlinear systems with prescribed performance," *IEEE Transactions on Fuzzy Systems*, vol. 28, no. 12, pp. 3161–3170, 2020.

[46] R. Zhang, B. Xu, and W. L. Zhao, "Finite-time prescribed performance control of MEMS gyroscopes," *Nonlinear Dynamics*, vol. 101, no. 4, pp. 2223–2234, 2020.

[47] T. W. Strganac, J. Ko, D. E. Thompson, and A. J. Kurdila, "Identification and control of limit cycle oscillations in aeroelastic systems," *Journal of Guidance, Control, and Dynamics*, vol. 23, no. 6, pp. 1127–1133, 2000.